Journal of
Mechanics of
Materials and Structures

AN APPROACH TO MODELING EXTREME LOADING OF STRUCTURES USING PERIDYNAMICS

Paul N. Demmie and Stewart A. Silling

Volume 2, Nº 10 December 2007

mathematical sciences publishers

JOURNAL OF MECHANICS OF MATERIALS AND STRUCTURES
Vol. 2, No. 10, 2007

AN APPROACH TO MODELING EXTREME LOADING OF STRUCTURES USING PERIDYNAMICS

PAUL N. DEMMIE AND STEWART A. SILLING

We address extreme loading of structures using peridynamics. The peridynamic model is a theory of continuum mechanics that is formulated in terms of integro-differential equations without spatial derivatives. It is a nonlocal theory whose equations remain valid regardless of fractures or other discontinuities that may emerge in a body due to loading. We review peridynamic theory and its implementation in the EMU computer code. We consider extreme loadings on reinforced concrete structures by impacts from massive objects. Peridynamic theory has been extended to model composite materials, fluids, and explosives. We discuss recent developments in peridynamic theory, including modeling gases as peridynamic materials and the detonation model in EMU. We then consider explosive loading of concrete structures. This work supports the conclusion that peridynamic theory is a physically reasonable and viable approach to modeling extreme loading of structures.

1. Introduction

In this paper, we address the extreme impact and explosive loading of structures using peridynamic theory, or *peridynamics*. The present paper is the first publication of results and developments in peridynamic theory to model extreme loading of large structures. Peridynamics is a theory of continuum mechanics that is formulated in terms of integro-differential equations without spatial derivatives [Silling 2000]. Conventional continuum-mechanics theory is formulated in terms of partial differential equations with spatial derivatives. However, these derivatives do not exist at discontinuities, and the conventional theory breaks down as a spatial discontinuity develops. Peridynamics replaces the spatial derivatives of conventional continuum-mechanics theory with integrals and assumes that particles in a continuum interact across a finite distance as in molecular dynamics. Therefore, an attractive feature of peridynamics is that its equations remain valid regardless of any fractures or discontinuities that may emerge in a structure due to loading. Implementation of peridynamics does not use stress intensity factors and does not require a separate law that tells cracks when and where to grow. Cracks emerge spontaneously as a result of the equations of motion and material model. They grow in whatever direction is energetically favorable for growth.

Although peridynamic theory is relatively new compared to conventional continuum-mechanics theory, its development is continuing and it has been applied to solve a number of problems. The method has origins in the work of Rogula [1982] and Kunin [1982] on nonlocal behavior in crystals.

Keywords: peridynamics, continuum mechanics, computational mechanics, solid mechanics, deformation, fracture, extreme loading.

Sandia National Laboratories is a multiprogram laboratory operated by Sandia Corporation, a Lockheed Martin Company, for the United States Department of Energy under contract DE-AC04-94AL85000.

Silling [2000] expanded and developed the model as a general way to formulate initial-boundary value problems in which the spontaneous occurrence of discontinuities is important. He proposed the term "peridynamic" from the Greek roots for "near" and "force". He demonstrated that the reformulated approach permits the solution of fracture problems using the same equations either on or off the crack surface or crack tip without knowledge of the initial location of the crack. Since particles separated by a finite distance can interact with each other as in molecular dynamics, the theory is nonlocal. Although there are other nonlocal theories of continuum mechanics, they do not attempt to eliminate the spatial derivatives.

Silling [2003] described a numerical method for solving initial-value problems within peridynamic theory. Accuracy and numerical stability were addressed in [Silling and Askari 2005] This work also showed how to include nonhomogeneous materials, such as fiber-reinforced composite materials, as peridynamic materials.

Silling et al. [2003] applied peridynamics to study deformation of a peridynamic bar. Their solution exhibits features that are not present in the classical result but converges with the classical result in the limit of short-range forces. Gerstle and Sau [2004] and Gerstle et al. [2005] applied peridynamic theory to the quasistatic deformation of concrete. They illustrated the deformation and fracture of small plain concrete samples and the effect of using rebar reinforcement. Silling and Bobaru [2005] applied peridynamic theory to study stretching and tearing of membranes. They also studied string-like structures, similar to long molecules, that sustain tensile loads while interacting with each other through intermolecular and contact forces. Their work is an early effort to apply peridynamic theory at the nanoscale.

For several years, we have used peridynamic theory to investigate damage resulting from aircraft impacting buildings and other large structures made of reinforced concrete. In the present paper, we discuss this approach to modeling extreme loading of large structures. We also present some recent developments in peridynamics, which provide an approach to modeling loading from explosive detonations.

Since peridynamic theory is relatively new, we first review peridynamic theory. In Section 2, we state the fundamental integro-differential equation of peridynamic theory and introduce the pairwise force function (PFF). The PFF is the force per unit volume squared between two particles. This interaction is called a bond. Constitutive properties of a material are given by specifying the PFF. Thus, in peridynamics, material response, damage, and failure are determined at the bond level. Bond properties can be derived from material properties including elastic modulus, yield properties, and fracture toughness [Silling 2000].

After discussing some properties of the PFF, we discuss the material models that we use for extreme-loading analyses. These materials are called proportional, microelastic or microplastic materials. For these materials, failure of a bond occurs when the stretch exceeds a value called the critical stretch.

In Section 3, we discuss the numerical method used to solve the integro-differential equations of peridynamics in the EMU computer code. In this section, we also review accuracy and stability for explicit time integration. EMU is the first computer code that is based on the peridynamic theory of continuum mechanics.

Section 4 contains a discussion of the EMU computer code. EMU is mesh free and Lagrangian. It uses explicit time integration to advance the solution in time and executes on parallel computers.[1]

[1] Information on EMU can be found at www.sandia.gov/emu/emu.htm.

In Section 5, we consider impacts of aircraft into reinforced concrete structures. We first discuss a simulation of an experiment that was performed at Sandia National Laboratories. In the test, an F4-Phantom impacted a massive, essentially rigid reinforced concrete wall [Sugano et al. 1993]. Because of the strength of the target, there was no perforation of the target. In the second example, there is perforation. An aircraft impacts a cylindrical structure made of reinforced concrete. In this example, we demonstrate the ability of peridynamics to model deformation and fracture leading to perforation. The ability to model fracture in perforation problems is important since a target starts to weaken long before a penetrator gets through and the fracture growth process determines fragment properties.

We next focus on explosive loading. Before introducing the EMU detonation model, we describe modeling gases as peridynamic materials in Section 6 since the detonation products are gases. How to model fluids as peridynamic materials is particularly important since the pairwise interactions through the linearized PFF imply a Poisson's ratio of $1/4$ [Silling 2000]. We describe the EMU detonation model in Section 7.

In Section 8, we consider explosive loading of a spherical shell and a large reinforced concrete structure containing water.

Section 9 contains a summary and conclusions of this work. There, we also discuss current work and future directions in the development and applications of peridynamic theory and the EMU computer code.

2. Peridynamic theory and material modeling

Consider a peridynamic body that occupies a domain R as shown in Figure 1.

In the peridynamic theory, the force density on a particle at point $\boldsymbol{x}$ and time t is assumed to be given by

$$\rho(\boldsymbol{x})\frac{d^2}{dt^2}\boldsymbol{u}(\boldsymbol{x},t) = \iiint_R \boldsymbol{f}\big(\boldsymbol{u}(\boldsymbol{x}',t)-\boldsymbol{u}(\boldsymbol{x},t),\boldsymbol{x}'-\boldsymbol{x}\big)dV' + \boldsymbol{b}(\boldsymbol{x},t), \tag{1}$$

where $\rho(\boldsymbol{x})$ is the density at $\boldsymbol{x}$, $\boldsymbol{x}$ and $\boldsymbol{x}'$ are points in the reference configuration, t is the time, $\boldsymbol{u}$ is the displacement vector, R is the domain of the body, $\boldsymbol{f}$ is the pairwise force function, and $\boldsymbol{b}$ is the

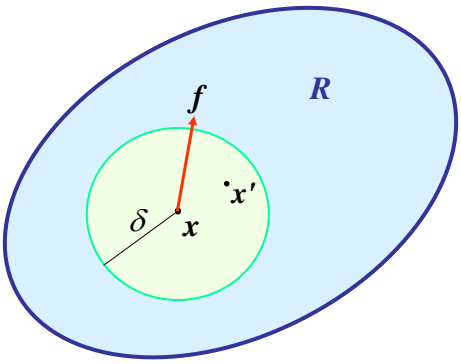

Figure 1. A peridynamic body occupying a domain R.

body-force density. (In Equation (1) and elsewhere, bold quantities are vectors unless stated otherwise.) The integral in Equation (1) is taken over the volume occupied by R. All functions are assumed to be sufficiently well behaved that the integral exists.

Equation (1) is the fundamental integro-differential equation of peridynamic theory. It is based on Newton's second law for all points within the domain of analysis. It does not contain any spatial derivatives. The specific force term is a functional depending on a vector-valued function, $\boldsymbol{f}$, called the pairwise force function (PFF). The PFF gives the force per unit volume squared on a particle at $\boldsymbol{x}$ due to a particle at $\boldsymbol{x}'$. In conventional continuum-mechanics theory, this functional is the divergence of the stress tensor. All constitutive properties of a material are given by specifying the PFF.

Figure 1 shows a sphere $S_\delta(\boldsymbol{x})$ of radius δ centered at the point $\boldsymbol{x}$. It is convenient to assume that there is a distance δ such that the PFF function vanishes outside $S_\delta(\boldsymbol{x})$ for each point $\boldsymbol{x}$ in the domain of analysis. The quantity δ is called the *horizon* since a particle cannot "see" a force beyond its horizon. This assumption is natural for the types of materials that are used for extreme-loading analysis as discussed below. It is also reasonable for forces that die off sufficiently rapidly or become shielded by intervening particles.

The appropriate value of δ depends on the physical nature of the application. At the nanoscale, it is determined by the distance over which physical interactions between atoms or molecules occur. At the macroscale, it is somewhat arbitrary since, for any given value of δ, the parameters in the PFF can be chosen to match the bulk-elastic properties of the material, as well as its most important fracture properties [Silling and Askari 2005]. However, in numerical modeling, typically δ is chosen to be three times the grid spacing. Values much smaller than this value result in undesirable grid effects such as cracks growing along the rows or columns of the grid. Values much larger than this may result in excessive wave dispersion and computational time.

Several properties of materials follow from the form of the PFF in (1). First, the dependence of $\boldsymbol{f}$ on $\boldsymbol{x}-\boldsymbol{x}'$ implies that the materials are homogeneous. Here, we will not consider extensions of peridynamic theory for nonhomogeneous materials. Second, the materials have no memory of their deformation history. Modeling materials with memory is a potential area for future research and development of peridynamic theory. Perhaps the fractional calculus [Oldham and Spanier 1974] can be useful since the fractional calculus has been useful for rheology of materials with memory (see articles in [Hilfer 2000]).

Consider the functional dependence of PFF shown in (1). It is convenient to express the PFF in terms of the new set of variables, $\boldsymbol{\xi}$ and $\boldsymbol{\eta}$, where

$$\xi = \boldsymbol{x}' - \boldsymbol{x} \qquad \text{and} \qquad \boldsymbol{\eta} = \boldsymbol{u}(\boldsymbol{x}', t) - \boldsymbol{u}(\boldsymbol{x}, t). \tag{2}$$

$\boldsymbol{\xi}$ is the relative position of particles at $\boldsymbol{x}$ and $\boldsymbol{x}'$ in the reference configuration and $\boldsymbol{\eta}$ is the difference in displacements at these points.

Figure 2 illustrates the relationship among the variables introduced thus far.

In this figure and elsewhere, $\boldsymbol{u}' = \boldsymbol{u}(\boldsymbol{x}', t)$. From this figure, $\boldsymbol{\eta}+\boldsymbol{\xi}$ is the relative position of the particles originally at $\boldsymbol{x}$, $\boldsymbol{x}'$ in the deformed configuration.

In terms of the new variables $\boldsymbol{\eta}$ and $\boldsymbol{\xi}$, the PFF $\boldsymbol{f}$ becomes

$$f\big(\boldsymbol{u}(\boldsymbol{x}', t) - \boldsymbol{u}(\boldsymbol{x}, t), \boldsymbol{x}' - \boldsymbol{x}\big) = \boldsymbol{f}(\boldsymbol{\eta}, \boldsymbol{\xi}). \tag{3}$$

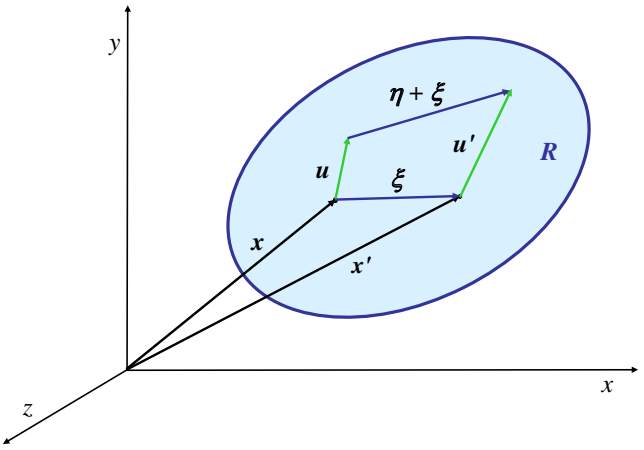

Figure 2. Relationships among the variables.

Newton's laws not only lead to the fundamental equation of peridynamics but also imply another property of the PFF $\boldsymbol{f}$. Newton's third law states that the force on a particle at $\boldsymbol{x}$ due to a particle at $\boldsymbol{x}'$ must be the negative of the force on a particle at $\boldsymbol{x}'$ due to a particle at $\boldsymbol{x}$. Therefore for (1) to satisfy Newton's third law, $\boldsymbol{f}(\boldsymbol{\eta}, \boldsymbol{\xi})$ must satisfy

$$\boldsymbol{f}(-\boldsymbol{\eta}, -\boldsymbol{\xi}) = -\boldsymbol{f}(\boldsymbol{\eta}, \boldsymbol{\xi}), \quad \text{for all } \boldsymbol{\eta}, \boldsymbol{\xi}. \tag{4}$$

Thus, $\boldsymbol{f}(\boldsymbol{\eta}, \boldsymbol{\xi})$ is an odd function of $(\boldsymbol{\eta}, \boldsymbol{\xi})$.

The next property of the PFF follows from the requirement to conserve angular momentum in the absence of external forces. If angular momentum were not conserved, then two particles initially at rest would move even in the absence of external forces. Thus, to ensure conservation of angular momentum, $\boldsymbol{f}(\boldsymbol{\eta}, \boldsymbol{\xi})$ must satisfy

$$(\boldsymbol{\eta} + \boldsymbol{\xi}) \times \boldsymbol{f}(\boldsymbol{\eta}, \boldsymbol{\xi}) = 0, \quad \text{for all } \boldsymbol{\eta}, \boldsymbol{\xi}, \tag{5}$$

where "$\times$" is the cross product. This expression implies that the force between any two particles must be parallel to their current relative position. Therefore, (5) implies that $\boldsymbol{f}(\boldsymbol{\eta}, \boldsymbol{\xi})$ must have the functional form

$$\boldsymbol{f}(\boldsymbol{\eta}, \boldsymbol{\xi}) = F(\boldsymbol{\eta}, \boldsymbol{\xi})(\boldsymbol{\eta} + \boldsymbol{\xi}), \quad \text{for all } \boldsymbol{\eta}, \boldsymbol{\xi}, \tag{6}$$

where F is a scalar-valued function. Since $\boldsymbol{f}(\boldsymbol{\eta}, \boldsymbol{\xi})$ is an odd function of $(\boldsymbol{\eta}, \boldsymbol{\xi})$, $F(\boldsymbol{\eta}, \boldsymbol{\xi})$ must be an even function of $(\boldsymbol{\eta}, \boldsymbol{\xi})$.

Gravity is important to determine the long-term consequences of impacts to structures. Before continuing the discussion of material modeling in peridynamics, we note that gravity is included in (1) as a body-force density. The body-force density for gravity, $\boldsymbol{b}_{\text{gravity}}$ is given by

$$\boldsymbol{b}_{\text{gravity}} = \rho(\boldsymbol{x})\boldsymbol{g}, \tag{7}$$

where $\boldsymbol{g}$ is the acceleration vector due to gravity with magnitude $\boldsymbol{g} = 9.814\,\text{m/s}^2$.

In the previous discussion, we showed that Newton's third law and the physical requirement to conserve angular momentum in the absence of external forces imply that the PFF must be in the direction of the relative displacement in the deformed configuration as given by (6). Here, we develop the general

form of the PFF for materials that are used in loading analyses. Although many of these results were first published in [Silling 2000], we provide this short summary and discussion for completeness and to provide results that are used in Section 6 to model gases as peridynamic materials.

All constitutive properties of a material are given by specifying the PFF. Previously, we showed that the dependence of the PFF $\boldsymbol{f}$ on $\boldsymbol{\xi}$ implies that the material is homogeneous. If a material is isotropic, then there is a further restriction on the functional dependence of $\boldsymbol{f}$. Proper behavior of $\boldsymbol{f}$ under the orthogonal rotation group in three dimensions implies that F in (6) must be invariant under this group. Hence, the scalar function F depends only on the length of $\boldsymbol{\eta}$, the angle between $\boldsymbol{\eta}$ and $\boldsymbol{\xi}$, and the length of $\boldsymbol{\xi}$. However, we find it more convenient to use the length of $\boldsymbol{\eta}+\boldsymbol{\xi}$ rather than $\boldsymbol{\eta}$. Therefore, for isotropic materials, the most general form for F is

$$F(\boldsymbol{\eta}, \boldsymbol{\xi}) = I(p, q, r), \quad \text{where } p = |\boldsymbol{\eta}+\boldsymbol{\xi}|,\ q = \boldsymbol{\eta}\cdot\boldsymbol{\xi},\ \text{and } r = |\boldsymbol{\xi}|, \tag{8}$$

where I is some scalar-valued function and "$\cdot$" is the dot product.

A peridynamic material is said to be *microelastic* if and only if there exists a scalar-valued function $w(\boldsymbol{\eta}, \boldsymbol{\xi})$ such that

$$\boldsymbol{f}(\boldsymbol{\eta}, \boldsymbol{\xi}) = \frac{\partial w}{\partial \boldsymbol{\eta}}(\boldsymbol{\eta}, \boldsymbol{\xi}). \tag{9}$$

The function w is called the *micropotential*. It is important to realize that the derivatives in (9) are not the spatial derivatives that are to be avoided by using peridynamic theory.

The micropotential has units of energy per unit volume squared. It represents potential energy density associated with a bond. We may define a functional that for a displacement $\boldsymbol{u}$ is the *local displacement energy density*,

$$W_u(\boldsymbol{x}, t) = \frac{1}{2}\iiint_R w(\boldsymbol{u}' - \boldsymbol{u}, \boldsymbol{x}' - \boldsymbol{x})\, dV'. \tag{10}$$

Equation (10) is the energy density at the point $\boldsymbol{x}$ and time t associated with a displacement $\boldsymbol{u}$ of all the particles in domain R. The factor of $1/2$ is present since only half the energy is associated with each endpoint of the bond.

Integration of (10) over the body yields the *total macroscopic energy* functional. Silling [2000] showed that the time rate of change of the kinetic energy plus the time rate of change of the total macroscopic energy given by the integral of (10) over the body equals the work on the body done by external forces when the fundamental equation of peridynamics (1) is satisfied.

The most general form of the PFF $\boldsymbol{f}$ for a microelastic material is

$$\boldsymbol{f}(\boldsymbol{\eta}, \boldsymbol{\xi}) = H(p, \boldsymbol{\xi})(\boldsymbol{\eta}+\boldsymbol{\xi}) \quad p = |\boldsymbol{\eta}+\boldsymbol{\xi}|, \tag{11}$$

where H is a scalar-valued function of $(p, \boldsymbol{\xi})$. In this case, there is a micropotential $w(p, \boldsymbol{\xi})$ such that

$$H(p, \boldsymbol{\xi}) = \frac{1}{p}\frac{\partial w}{\partial p}(p, \boldsymbol{\xi}). \tag{12}$$

The form of $\boldsymbol{f}$ in (11) implies that the force between any two points depends only on the distance between them in the deformed configuration. Thus, we may interpret a microelastic material as a material in which each two points is connected by a spring that, in general, may be nonlinear. If a microelastic material is isotropic, then (8) implies that H and w only depend on p and r, the magnitude of $\boldsymbol{\xi}$.

The final specialization on the PFF that we will adopt is a further development of the notion that particles in microelastic materials may be considered to be connected by springs. We consider materials with a PFF having its magnitude proportional to the stretch s, where

$$s = \frac{p - r}{r}, \quad p = |\boldsymbol{\eta} + \boldsymbol{\xi}|, \text{ and } r = |\boldsymbol{\xi}|. \tag{13}$$

Materials having magnitudes proportional to the stretch are called *proportional* materials. The most general form of the PFF for proportional, microelastic materials is

$$\boldsymbol{f}(\boldsymbol{\eta}, \boldsymbol{\xi}) = \frac{g(s, r)}{p}(\boldsymbol{\eta} + \boldsymbol{\xi}), \tag{14}$$

where $g(s, r)$ is a piecewise linear function of s. The function g is called the *bond force* between two particles for a microelastic, proportional peridynamic material. Figure 3 shows the bond force dependence on bond stretch for such materials. This figure also shows the bond force for a *microplastic* material. The behavior of peridynamic microelastic and microplastic materials differ only on unloading. A microelastic material unloads reversibly back to zero stretch, while a microplastic material that is stretched beyond the elastic limit will retain some stretch when unloaded.

Figure 3 shows a linear dependence with nonzero slope in the elastic regime and constant bond force when the yield strength magnitude is exceeded in tension or compression. This figure also indicates bond failure at some value of bond stretch. Proportional peridynamic materials fail irreversibly when the stretch exceeds a value, s_c, called the *critical stretch*. Not only does the critical stretch define failure of a material, but it also assures the existence of a horizon for proportional materials. A microelastic, proportional material behaves reversibly as long as the stretch does not exceed the critical stretch.

Let $V_d(\boldsymbol{x}, t)$ denote the volume of the material that connected to $\boldsymbol{x}$ by bonds that have been broken and $V_0(\boldsymbol{x})$ denote the volume of material initially connected to $\boldsymbol{x}$. Then the *damage* $D(\boldsymbol{x}, t)$ is defined by

$$D(\boldsymbol{x}, t) = V_d(\boldsymbol{x}, t)/V_0(\boldsymbol{x}). \tag{15}$$

3. Numerical method

To solve the fundamental peridynamics equation of motion, (1), the domain is discretized into a set of nodes, $\{\boldsymbol{x}_i\}$, as depicted in Figure 4. Each node has a known volume in the reference configuration. The nodes form a computational grid.

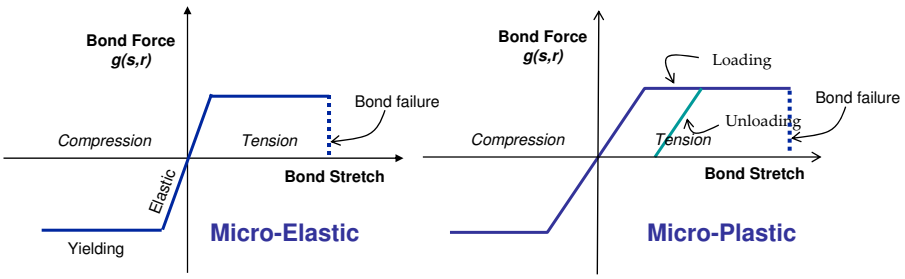

Figure 3. Bond force for microelastic and microplastic proportional materials.

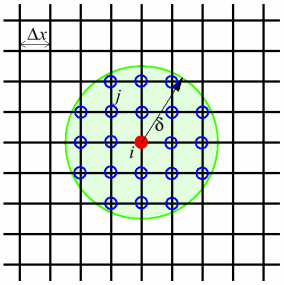

Figure 4. Computational grid.

The fundamental equation of motion (1) is replaced by a finite sum, which at time t_n is

$$\rho_i \frac{d^2}{dt^2}\boldsymbol{u}_i^n = \sum_p \boldsymbol{f}(\boldsymbol{u}_p^n - \boldsymbol{u}_i^n, \boldsymbol{x}_p - \boldsymbol{x}_i)V_p + \boldsymbol{b}_i^n, \tag{16}$$

where $\rho_i = \rho(\boldsymbol{x}_i)$, $\boldsymbol{u}_i^n = \boldsymbol{u}(\boldsymbol{x}_i, t_n)$, $\boldsymbol{b}_i^n = \boldsymbol{b}(\boldsymbol{x}_i, t_n)$, and V_p is the volume of node p. The sum is taken over all nodes within the horizon δ of x_i, $\{x_p : |x_p - x_i| < \delta\}$.

The acceleration term in (16) is approximated by an explicit central difference:

$$\boldsymbol{u}_i^n = \frac{\boldsymbol{u}_i^{n+1} - 2\boldsymbol{u}_i^n + \boldsymbol{u}_i^{n-1}}{(\Delta t)^2}, \tag{17}$$

where Δt is the constant time step. The error in (17) is well known to be second order in time [Silling and Askari 2005].

Silling and Askari [2005] investigated the accuracy of (16) with grid spacing and stability for a linearized PFF, where

$$\boldsymbol{f}(\boldsymbol{\eta}, \boldsymbol{\xi}) = \boldsymbol{C}(\boldsymbol{\xi})\boldsymbol{\eta}, \quad \text{where } \boldsymbol{C}(\boldsymbol{\xi}) = \frac{\partial \boldsymbol{f}(0, \boldsymbol{\xi})}{\partial \boldsymbol{\eta}}. \tag{18}$$

In (18), $\boldsymbol{C}(\boldsymbol{\xi})$ is called the *micromodulus*. The micromodulus is a second order tensor or 3×3 matrix. They showed that if the micromodulus and displacement $\boldsymbol{u}$ are twice continuously differentiable, then (16) is second-order accurate in grid spacing. Otherwise, if there are discontinuities in $\boldsymbol{C}$ or $\boldsymbol{u}$, (16) is first-order accurate in grid spacing. They also presented a stability criterion for the time step Δt, which states that the maximum time step is of order of the horizon. Hence, the maximum stable time step is limited by the horizon rather than the grid spacing. Alternative approaches to integrating the peridynamic equation of motion, along with some important mathematical properties of one-dimensional solutions, are discussed by Weckner and Abeyaratne [2005] and Emmrich and Weckner [2007].

4. The EMU computer code

EMU is the first computer code that is based on the peridynamic theory of continuum mechanics. It is written in Fortran 90 and executes on computers operating under Unix/Linux or Windows operating systems and on parallel computers using MPI (message passing interface). EMU is currently in the research and development stage and is being licensed to a few users.

The numerical method described in Section 3 does not use elements, and there are no geometrical objects connecting the grid points. Hence, EMU is mesh free. There is no need for a mesh generator when modeling complex structures. Only the generation of grid points is required.

EMU is Lagrangian in the sense that each node contains a fixed amount of material. A body contains multiple nodes and may fragment if bonds between nodes are broken. However, the mass in each node remains constant.

EMU uses explicit time integration to advance the solution in time as discussed in Section 3. Explicit time integration is a simple, reliable method. A stable time-step estimate was obtained by Silling and Askari [2005] for a linear PFF as given by (18). For nonlinear materials, a safety factor less than one may be applied to this stable time step to account for possible nonlinear material response that would make the estimated stable time step based on the linear analysis too large.

Execution of an EMU simulation requires a computational grid and an input file containing data to control execution, provide information on the grid geometry, and specify material properties. (An unpublished user's manual is available to licensed users of EMU.)

A computation grid in EMU can be defined in either of two ways, or any combination of the two. Figure 5 shows an EMU problem containing two internally generated material regions and one externally generated grid. Everything outside the material regions is empty space.

For an internally generated grid, the code currently uses a lattice inside a rectangular box. The box containing the lattice includes several material regions, each region with a given material. There are various options for defining the shapes of these regions. A lattice site that is inside one of the material regions becomes a node. A lattice site that is not in any material region represents a void and is, in effect, not used during the calculation.

For an externally generated grid, one typically writes a separate program to generate the grid point coordinates and material numbers and place them into files that are processed during EMU execution.

A user writes an input file containing data to control execution, specify details of the grid geometry, and specify material properties. After the title on the first line of the input file, the input is keyword based. The keywords may be placed in any order. Any numerical input following a keyword is format-free and may extend to multiple lines. SI units are recommended for all dimensional quantities. Data to control

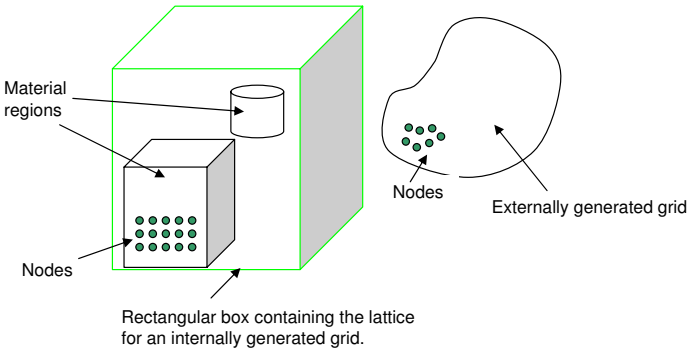

Figure 5. A computational grid containing two internally generated material regions and one externally generated region.

execution include time span or number of cycles for execution of a simulation, time-step safety factor, plot-dump frequency, and location of output files. Data to specify details of the grid geometry include grid spacing, horizon, and volume of a node for each material.

The details of the peridynamic material model are specified in the EMU input file. For each proportional, microelastic material, the user provides its density or total mass, yield strength, sound speed, and critical stretch. Alternately, material properties of microelastic materials may be specified by the penetrability as measured by Young's S-number [Young 1969]. Specific inputs give properties of fluids, gases, or explosive materials.

Initial and boundary conditions may be specified in the input file. Boundary conditions include fixed displacement or velocity and applied force. They are applied somewhat differently in the peridynamic method than in the classical approach. In peridynamics, boundary conditions are prescribed within a layer of finite thickness at the surface of a body. This layer must include some nodes in the computational grid. Forces at the surface of a body are applied as body force density $\boldsymbol{b}$ in (1) within some layer under the surface.

In peridynamics as implemented in EMU, contact is treated using short-range repulsive forces that prevent nodes from getting too close. These short-range forces are independent of the positions of the nodes in the reference configuration, so that contact is treated in a consistent way even under large deformations. This approach is physical and avoids the need for defining contact surfaces as is required by many finite-element codes.

EMU is parallelized using MPI and executes on parallel computers. Parallelization was performed by allowing each processor to be responsible for a fixed region of space. Figure 6 illustrates this processor partitioning in two dimensions.

Figure 6 shows a grid surrounded by a margin region, which is the light blue shaded area. The regions of space owned by the eight processors in this example are separated by heavy red lines. Each processor region owns the nodes within its domain and needs information from nodes a distance equal to the horizon δ surrounding its domain. As the body deforms, nodes are permitted to migrate between processors. After each time step, the updated variables for nodes within a distance δ of a given processor are passed using MPI subroutines to be used during the following cycle. This parallelization technique

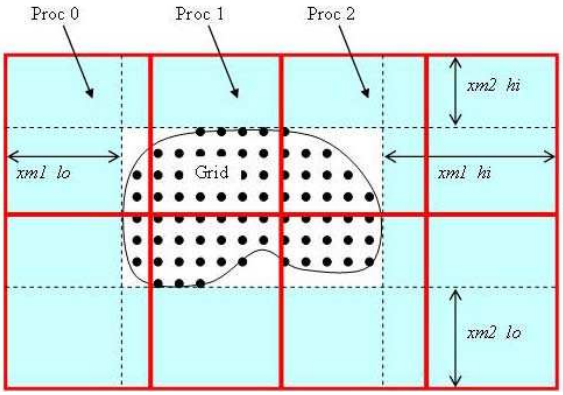

Figure 6. Computation grid and margin region partitioned among eight processors.

has the advantage of simplicity. However, load balancing is not optimal as seen in Figure 6 since the two processors along the right boundary do not process any nodes. More sophisticated load balancing methods will be considered as part of future development of EMU to improve efficiency in problems involving large displacements.

A graphics postprocessor was written to produce output that can be viewed or further processed into many graphics formats, such as JPG or encapsulated postscript, using the RSCORS graphics system [Padilla and Thompson 1984]. Postprocessing software is also available to plot displacement histories and fragmentation histories and distributions.

5. Examples of large objects impacting concrete structures

We consider two examples of aircraft impacts into reinforced concrete structures to illustrate the capability of EMU to model extreme impacts.

In the first example, we simulated a test that was performed at Sandia National Laboratories [Sugano et al. 1993]. In the test, an F-4 Phantom aircraft impacted an massive, essentially rigid reinforced concrete wall. The primary purpose of the test was to determine the impact force as a function of time for the impact of an F-4 Phantom. Additional objectives of the test were to determine the crushing behavior of the aircraft, to determine if the engines broke away from the aircraft before their impact, and if so, to measure their impact velocity, and to record the dispersal of fuel after impact. Water was used instead of jet fuel for this test. The target was a block of reinforced concrete 3.6576 m thick in the direction of impact and 7.0104 m square perpendicular to the impact direction. It was mounted on a platform. The impact was perpendicular to the target at a speed of 215 m/s. The impacting mass of the aircraft and fuel surrogate was slightly more that 18,000 kg. The length of the F-4 is about 1.7678 m.

Figure 7 shows a top and side view of materials in the EMU model at time zero and materials at 0.05 s and 0.09 s during the simulation of the experiment, and Figure 8 shows damage to the structure. The damage at a node is given by (15). It represents the fraction of bonds that are broken between this node and all nodes initially having bonds with it.

In Figure 7, the concrete is yellow and the rebar is green, the fuel is gold and the remaining colors are various parts of the aircraft. The simulation took about 36 minutes using 8 processors, and the time steps varied from 21 μs to 36 μs. The time simulated is about 0.09 s. The grid spacing is 0.229 m, and there are 36,244 nodes in the computational model.

There is no perforation of the target because of the target's strength. Only crush up of the aircraft occurs during the simulation, as was observed during the experiment.

Figure 8 shows side and front views of damage to the target impacted by the F-4. We did not show damage to the aircraft in this figure. Only the concrete and its rebar reinforcement are shown in Figure 8. This figure shows damage ranging from no damage (purple) to over 99% damage (orange). Although the target was not perforated, there is considerable damage on the impacted surface that extends to the interior. At 0.05 s, there is over 99% damage to a large part of the impacted surface, and by 0.09 s this damage leads to concrete falling away from the target.

Figure 9 shows a penetrator impacting a target. This figure illustrates why peridynamics is useful in penetration analysis. In this figure, a penetrator (red) impacts at target (blue), fracture occurs, and fragments are emitted from the nonimpacted side of the target.

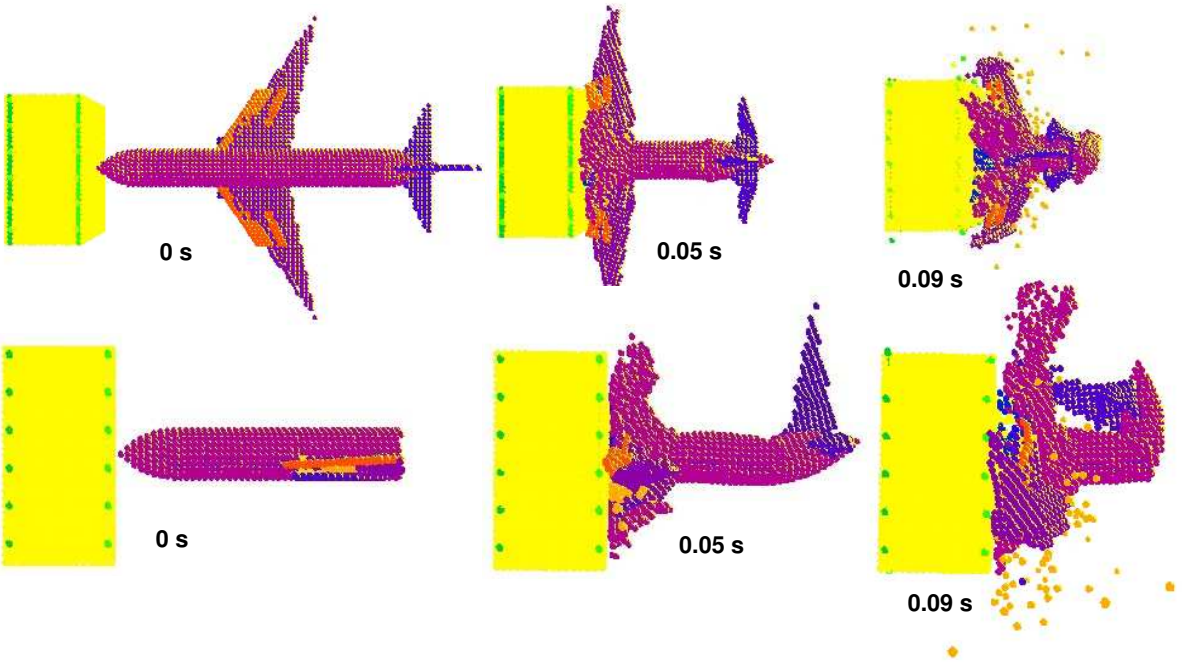

Figure 7. Top and side views of materials during F-4 impact simulation.

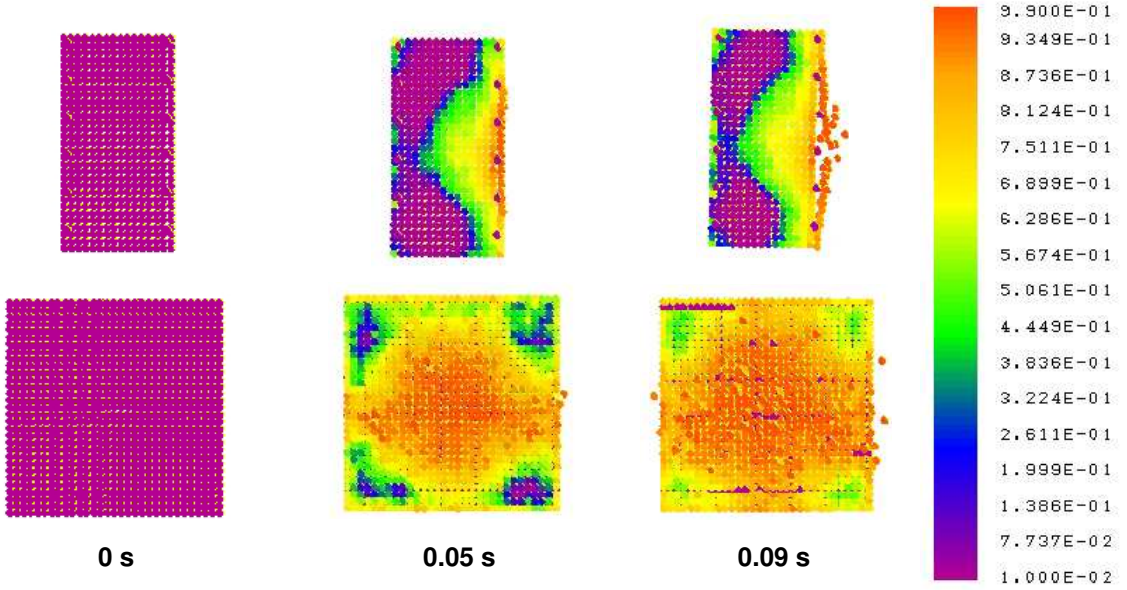

Figure 8. Side and front views of damage during F-4 impact simulation.

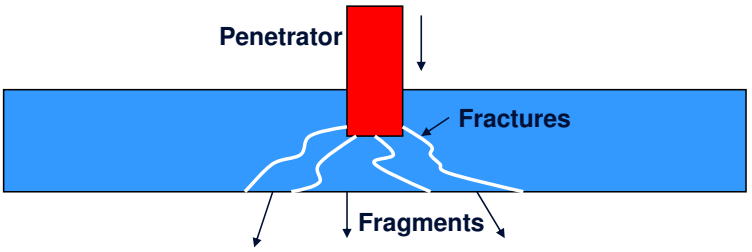

Figure 9. A penetrator impacting a target.

The ability to model fracture in perforation problems is important since fracture occurs before perforation occurs, as shown in Figure 9, and a target starts to weaken long before a penetrator gets through. Furthermore, the fracture process determines fragment properties, and fragments leaving a target may damage structures separated from the initial target.

For another example of the capabilities of peridynamics, consider an aircraft impacting a cylindrical structure made of reinforced concrete. The main part of the structure is a reinforced concrete cylinder with an inside radius 19.812 m, height 27.432 m, and wall thickness 0.9144 m. Rebar is placed in hoops coaxial with the cylinder axis and vertically parallel to the cylinder axis. The rebar is embedded in the concrete inside its inner and outer surfaces. The rebar is #18 rebar with 0.3048 m spacing. Rebar was omitted in the roof of the structure for simplicity since the roof concrete is in compression. The roof is 0.9144 m thick. The structure includes a 9.525 mm steel liner that is the color yellow in Figure 10 and coaxial with the concrete cylinder. The radius of the liner is 18.288 m. There is a 1.524 m annulus between the concrete and the steel liner.

Figure 10 shows results from the EMU simulation of this scenario. In this figure, the concrete is yellow and green and the rebar is orange, and the remaining colors are various parts of the aircraft including the jet fuel. The time simulated is about 0.64 s. The simulation took about 26.5 h using 64 processors, and the time steps varied from 13 μs to 20 μs. The grid spacing is 0.229 m, and there are 580,624 nodes in the computational model.

Figure 10 shows that before 0.17 s, the concrete wall is breached and the steel liner is deformed considerably. The breach in the concrete wall occurred soon after the hard parts of the aircraft, front landing gear, and center fuel tank (color green) impact the outer wall. By 0.64 s most of the aircraft is inside the structure. Only the tail end, parts of the wings, and some fuel from the wing tanks are not inside the structure. The center fuel tank remains intact.

Figure 11 shows the progression of internal damage to the structure starting at 0.10 s. This figure shows only the front half of the structure so that a breach will not be obscured by the back of the structure. At 0.10 s, fracturing and cracks in the concrete are evident and over 99% of the bonds are broken near the impact location. Much failure occurs along the rebar. However, there is cracking in the concrete along diagonals beginning where rebars intersect. Damage appears to occur first in the rebar, and the rebar seems to fail completely before the concrete fails.

Although there is much damage at 0.10 s, the concrete and liner are not penetrated. There are a few small holes in the structure near the impact location. Breech of the concrete wall and liner occur before 0.18 s as the concrete continues to fracture and the liner is torn. After 0.34 s, the breach gets wider as

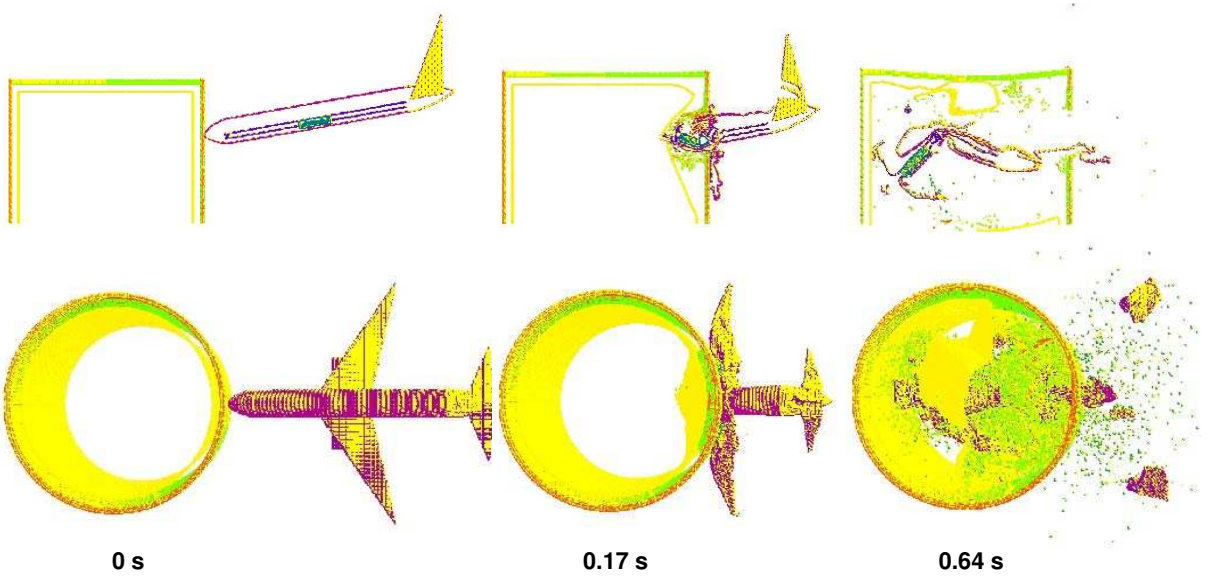

Figure 10. Side and top views of materials during simulation of an aircraft impacting a cylindrical concrete structure.

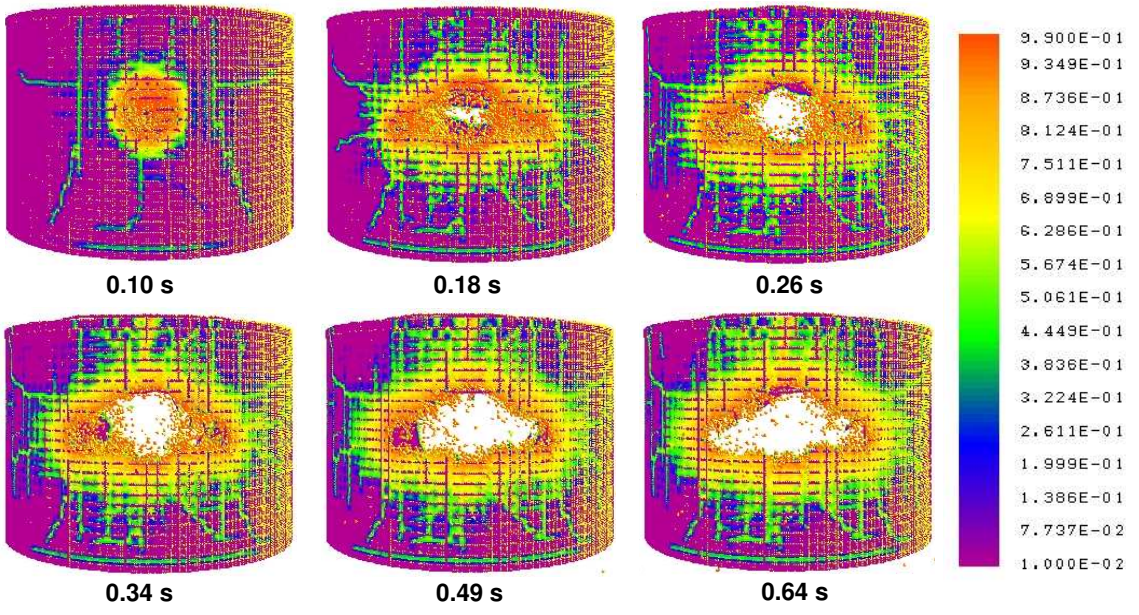

Figure 11. Damage to front of structure during simulation of an aircraft impact into a reinforced concrete structure.

parts of the wing penetrate and enter the structure. At the end of the simulation, over half of the front part of the structure is damaged.

The results in Figure 11 show the power of the peridynamics method in problems where deformation and fracture are expected. This figure shows the dynamic evolution of fracture with cracks emerging spontaneously as a result of the equations of motion and material model, and growing in whatever direction is energetically favorable for growth.

6. Gases as peridynamic materials

Since the detonation products in an explosion are gases, we must determine how to model gases as bond-based, peridynamic materials. In this section, we develop a general expression for the PFF of a gas. This expression depends on how the internal energy per unit volume of the gas changes with the expansion of the gas, X, where

$$X = \frac{v}{v_0} = \frac{\rho_0}{\rho}. \tag{19}$$

In (19), v and v_0 are the deformed and reference specific volumes of the gas, respectively, and ρ and ρ_0 are the deformed and reference densities, respectively. Implementation of a gas model requires approximating the expansion at a node from the undeformed and deformed bond lengths between this node and all gas nodes within its horizon. We provide the expression for the expansion that is presently used in EMU and complete this discussion of gases as peridynamic materials by developing the PFF for a gas.

To derive a general expression for the PFF of a gas, consider (9) and (10). From (9), the micropotential, w, may be written as

$$w(\boldsymbol{x}, t) = \int_{\boldsymbol{\eta}_0}^{\boldsymbol{\eta}(x,t)} \boldsymbol{f}(\boldsymbol{\eta}, \boldsymbol{\xi}) \cdot d\boldsymbol{\eta}, \tag{20}$$

where $\boldsymbol{\eta}_0$ is some fiducial state of stretch for evaluation of the micropotential. Since the integral (10) vanishes outside the horizon of $\boldsymbol{x}$, $H(\boldsymbol{x})$, (10) may be written using (20) as

$$W_u(\boldsymbol{x}, t) = \frac{1}{2} \iiint_{H(x)} \left[\int_{\boldsymbol{\eta}_0}^{\boldsymbol{\eta}(x',t)} \boldsymbol{f}(\boldsymbol{\eta}, \boldsymbol{\xi}) \cdot d\boldsymbol{\eta} \right] dV_\xi. \tag{21}$$

Let all the bonds be held fixed except for bond k at a given value of $\boldsymbol{\xi}$. Then, for an incremental stretch dp_k in bond k, (21) becomes dW, where

$$dW = \frac{1}{2} \boldsymbol{f} \cdot d\boldsymbol{\eta} \Delta V_\xi = \frac{1}{2} \boldsymbol{f} \cdot d(\boldsymbol{\eta} + \boldsymbol{\xi}) \Delta V_\xi = \frac{1}{2} \boldsymbol{f}_k dp_k \Delta V_k. \tag{22}$$

In (22), f_k is the magnitude of the bond force per unit volume squared in bond k due to this incremental stretch dp_k in this bond, and ΔV_ξ and ΔV_k are volume elements associated with bond k. The later two equalities follow since $\boldsymbol{\xi}$ is fixed under the stretch and $\boldsymbol{f}$ is parallel to $\boldsymbol{\eta} + \boldsymbol{\xi}$ as stated in (6).

The quantity f_k in (22) is the PFF for a gas. This quantity can be expressed in terms of the expansion X as follows.

Changes in the energy per unit volume, dW, result from the stretch dp_k. Therefore, using the definition of dW and the chain rule, (22) may be written as

$$dW = \frac{\partial W}{\partial p_k} dp_k = \frac{dW}{dX} \frac{\partial X}{\partial p_k} dp_k \tag{23}$$

since W depends on p_k through its dependence on X.

Equating (22) and (23) and solving for f_k yields a general expression for the PFF of a gas

$$f_k = \frac{2}{\Delta V_k} \frac{dW}{dX} \frac{\partial X}{\partial p_k}. \tag{24}$$

The PFF can be obtained from (24) once the energy per unit volume, W, is known as a function of the expansion, X, and X is known as a function of the incremental stretches for all gas bonds within the horizon of a node.

There are many ways to approximate the expansion X. The present discussion describes the method currently implemented in EMU. Consider the ratio of the deformed density to the reference density. This ratio is $1/X$. We approximate the ratio of the deformed to reference density at a given node by

$$\frac{1}{X} = \left[\frac{1}{V} \sum_j \left(\frac{r_j}{p_j} \right)^m \Delta V_j \right]^{3/m}, \quad V = \sum_k \Delta V_k, \tag{25}$$

where the sum is taken over the nodes inside the horizon of the given node, $p_j = |\boldsymbol{\eta}_j + \boldsymbol{\xi}_j|$, $r_j = |\boldsymbol{\xi}_j|$, and ΔV_j is the reference volume of node j. We refer to the nodes inside the horizon of a given node as its family. Hence, V is the total reference volume of the family of the given node.

If $m = 1$ and the reference-node volumes are equal, (13) implies that the summation in (25) represents the cube of the average of the inverses of the one plus bond stretches within the family. For $m > 0$ with constant bond stretch s, (25) implies that the relative density $1/X$ is

$$\frac{1}{X} = \frac{1}{(1+s)^3}. \tag{26}$$

As expected, (26) shows that the density increases in compression ($s < 0$) and decreases in expansion ($s > 0$). The purpose of including $m \neq 1$ in (25) is to allow for the possibility that bonds of different length could sustain different forces even if the deformation is an isotropic expansion. This form can be helpful, for example, in preventing nodes in a numerical grid from getting so close to each other that they overlap.

For any m and equal reference-node volumes, (25) becomes

$$\frac{1}{X} = \left[\frac{1}{N} \sum_j \left(\frac{1}{(1+s_j)} \right)^m \right]^{3/m}, \quad s_j = \frac{p_j - r_j}{r_j}. \tag{27}$$

Since (27) represents the ratio of deformed to reference density, the more highly compressed bonds ($s_j < 0$) will have a larger contribution to the overall density ratio at a node for $m > 1$.

From Equation (25), the expansion X is

$$X = \left[\frac{1}{V} \sum_j \left(\frac{p_j}{r_j} \right)^{-m} \Delta V_j \right]^{-3/m}, \quad V = \sum_k \Delta V_k. \tag{28}$$

From (24) with this approximation for the expansion, the PFF for a gas is

$$f_k = \frac{6}{r_k V} \frac{dW}{dX} \left(\frac{p_k}{r_k} \right)^{-m-1} X^{1+m/3}. \tag{29}$$

If we identify W with the internal energy per unit volume of the gas, then (29) and knowledge of the dependence of W on the expansion X yield an expression for the PFF at node k.

From an axiomatic formulation of thermodynamics, such as found in [Callen 1960], the pressure is an intensive variable defined as minus the partial derivative of the internal energy with respect to a specific volume at constant entropy [Callen 1960, p. 31]. Therefore, the derivative in (29) is

$$\frac{dW}{dX} = -P, \tag{30}$$

which implies that the PFF for node k in a gas is

$$f_k = -\frac{6P}{r_k V} \left(\frac{p_k}{r_k} \right)^{-m-1} X^{1+m/3}. \tag{31}$$

Implementation of (31) requires knowledge of P as a function of X and a value for m. In the current version of EMU, a value of $m = 1$ is used. We have not investigated the consequences of using different values for m or using some alternate formulation of the expansion.

For many applications of interest, gases are rapidly expanding. Therefore, in the initial implementation of gas modeling in EMU, gases are treated as ideal gases undergoing an isentropic or adiabatic expansion. In this case, we can relate the pressure required in (31) to the expansion.

Consider an isentropic process from a state with volume and temperature (V_0, T_0) to a state with volume and temperature (V, T). The change in entropy, ΔS, for an ideal gas between these states is given by

$$\Delta S = nR \ln \frac{V}{V_0} + nC_V \ln \frac{T}{T_0}, \tag{32}$$

where n is the number of moles of the gas, R is the gas constant (8.31 J/mol/K), and C_V is the molar specific heat at constant volume [Halliday et al. 2001, p. 487]. Setting $\Delta S = 0$ in (32) and using the ideal gas law ($PV = nRT$), we obtain the relation

$$PV^\gamma = P_0 V_0^\gamma, \tag{33}$$

where $\gamma = C_P/C_V$ is the ratio of molar specific heats and $C_P = C_V + R$ is the molar specific heat at constant pressure. Therefore, for an ideal gas, the pressure as a function of the expansion for an adiabatic expansion is given by

$$P = P_0 \left(\frac{V_0}{V} \right)^\gamma = P_0 X^{-\gamma}. \tag{34}$$

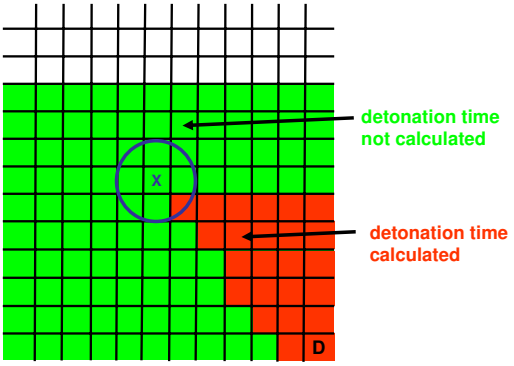

Figure 12. Huygen's construction procedure in two dimensions to calculate detonation times.

7. The peridynamic detonation model in EMU

A peridynamic detonation model was developed and implemented in the EMU computer code. The first component of the detonation model is the input. For each explosive material, the user provides the location of the detonation point ($\boldsymbol{x}_{\text{det}}$) and time of detonation initiation (t_{det}) along with the density of the unreacted explosive (ρ_{un}) and the detonation speed (V_{det}). Multiple detonation points are permitted in the current version of EMU. For an ideal gas, the user may also specify the pressure (P_{CJ}), ratio of molar specific heats (γ), and detonation temperature (T_{CJ}) of the detonation-product gases. If the user does not specify these quantities, they are obtained from the following correlations:

$$P_{CJ} = \rho_{un}(V_{\text{det}})^2\left[1.0 - 0.7125(\rho_{un}/1000)^{0.04}\right], \tag{35}$$

$$\gamma = 0.7125(\rho_{un}/1000)\left[1.0 - 0.7125(\rho_{un}/1000)^{0.04}\right], \tag{36}$$

$$T_{CJ} = 1643\gamma. \tag{37}$$

The units in (35), (36), and (37) are SI units; the ratio of molar specific heats (γ) is dimensionless [Cooper 1996, pp. 265, 79, and 156, respectively].

The next component of the detonation model is determining the detonation times at each node containing explosive material. These times are calculated during input processing using a Huygen's construction procedure. Since the detonation times are calculated during input processing, the method is called *program burn*. Figure 12 illustrates this procedure in two dimensions.

In Figure 12, the detonation is initiated in the node at the lower right cell labeled with a D. Detonation times have been calculated for the explosive material in the red cells and have not been calculated for the explosive material in the green cells. In this figure, the procedure started at the lower left and proceeded toward the right. After sweeping a row, the next row above is swept starting from the left. The procedure is currently in the green cell labeled with an X. While the idea of the construction is given by this discussion of Figure 12, the actual details differ somewhat during EMU execution since the nodes are not so well ordered in rows and columns as shown in this figure, and a node containing an explosive material may be owned by one processor and needed by another processor in the parallel implementation.

The detonation times are initially set to a large number. The construction proceeds by sweeping through the grid and examining at a given node X the detonation times of the nodes in a spherical

neighborhood of node X. If the node spacing is uniform with value Δq, then the radius of the spherical neighborhood is only slightly greater than $\sqrt{3}\Delta q$. Using this neighborhood radius ensures that the adjacent explosive nodes are not missed and that the detonation does not jump across a node that does not contain an explosive material. For any node X' in the neighborhood of node X, the detonation time for node X is the minimum of its detonation time and the detonation time of a node X' plus the time it takes the detonation to propagate from X' to X. This process continues until detonation times have been calculated for all explosive nodes. The Huygen's construction ensures that detonations propagate around obstacles and isolated regions of explosive material do not detonate.

When detonation occurs and the detonation products are ideal gases, the pressure of the gas is set to one half the Chapman–Jouguet pressure (P_{CJ}), which is given by (35) or specified by user input. To obtain the correct energy in the ideal-gas reaction products from the detonating explosive, the initial pressure must be set to one half the Chapman–Jouguet pressure. Once detonated, the gas expands adiabatically from this pressure. From (34), the pressure P at a time when the expansion is X is given by

$$P = \frac{1}{2} P_{CJ} \left(\frac{V_0}{V} \right)^{\gamma} = \frac{1}{2} P_{CJ} X^{-\gamma}. \tag{38}$$

With P given by (38), the PFF between gas nodes for an expansion X is given by (31).

The ideal gas law and (38) imply that the temperature T at a time when the expansion is X is

$$T = T_{CJ} \left(\frac{V_0}{V} \right)^{\gamma - 1} = T_{CJ} X^{-\gamma + 1}, \tag{39}$$

where T_{CJ} is given by (37) or specified by user input. The ratio of molar specific heats in (38) and (39) is given by (36) or specified by user input.

8. Examples of explosive loading of concrete structures

In this section, we illustrate the capability of EMU to model explosive loading by discussing two examples of explosive material detonating within concrete structures.

For the first example, consider a 0.05-m thick spherical concrete shell with an inside radius 0.25 m. The interior is filled with an explosive whose density is 1780 kg/m^3 and detonation speed is 8590 m/s. The explosive is detonated at time zero at the center of the sphere. Although this structure is not large, this problem was used to debug the detonation model.

We simulated about 200 μs of the explosion scenario. Using 2 processors, the simulation required about 0.76 h. The grid spacing is 0.01 m, and there are 133,185 nodes in the computational model.

Figure 13 is a cross section view of the materials at time zero and the calculated detonation times in the explosive. In the left graphic in this figure, the explosive is orange and the concrete is purple. The concrete is not reinforced. The detonation times in the right graphic vary from purple (less than 0.4 μs) to orange (greater than 40 μs). The calculated detonation times vary from 0 to about 35 μs. The orange applies to the concrete, which is not an explosive material.

Since peridynamic theory does not use stresses in its formulation, stress and pressure are not output during a simulation. Although temperature plays no role in the current models in EMU, a temperature field was included in the data model for future developments. The temperature field can be used to observe the propagation of the detonation, since upon detonation, the temperature is given by (37) or

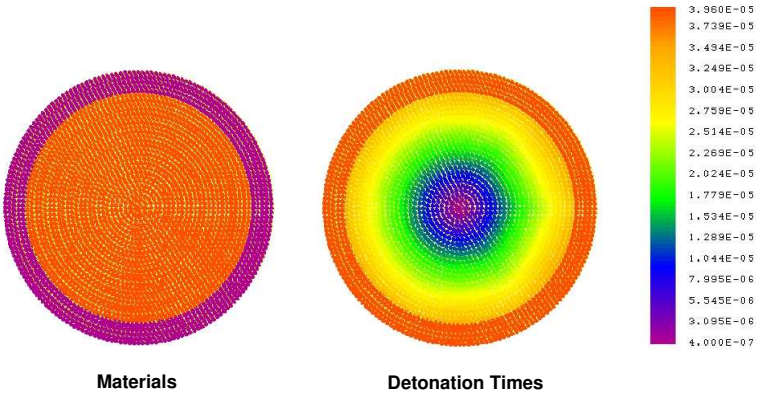

Figure 13. Materials at time zero and detonation times for exploding concrete shell.

user input and subsequently decreases during the adiabatic expansion as given by (39). Figure 14 shows temperatures calculated during the simulation of the explosion loading of the concrete shell.

Figure 14 shows the detonation propagating from shortly after initiation (1.4 μs) to 35 μs when all the explosive has detonated. The temperatures are in K.

At detonation, the temperature of the detonation products is about 4400 K. As the gas expands adiabatically, its temperature decreases as shown in the figure. The initial temperature of the concrete shell is 293 K. The temperature of the concrete will always be 293 K since there is no heat transfer mechanism

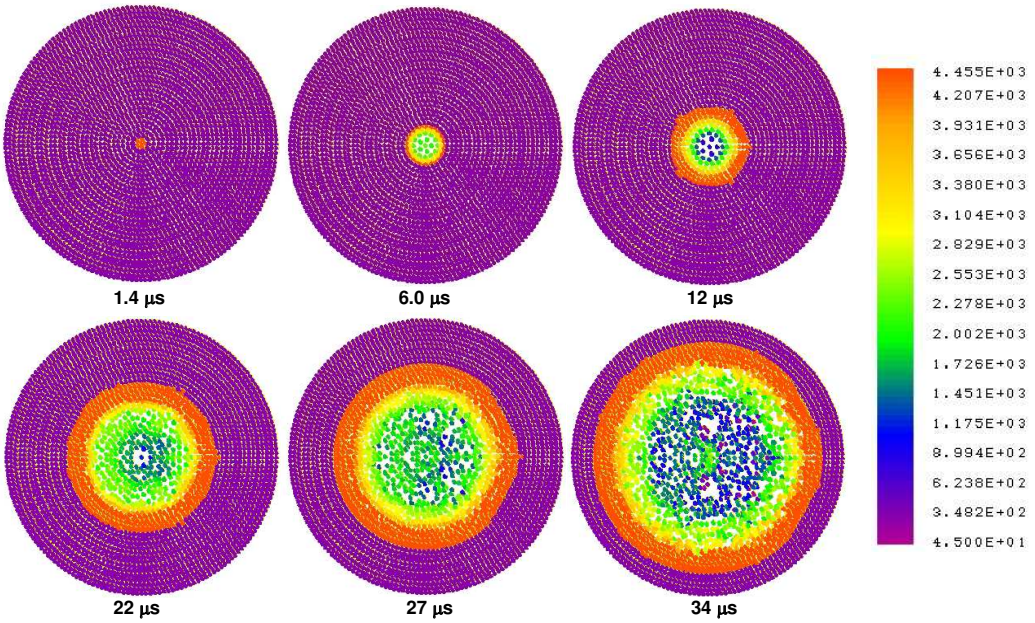

Figure 14. Temperatures showing propagation of the detonation for an exploding concrete shell.

in the current version of EMU. No distortion of the concrete shell is evident during the times shown in Figure 14. Later times must be shown to observe expansion and damage to the shell.

Figure 15 shows materials during the simulation. To observe voids and damage as the detonation propagates, this figure contains only a 2-cm slice about the center of the sphere. This figure shows materials and indicates the progression of damage to the shell during the simulation. The graphics at 13 μs, 23 μs, and 35 μs show voids produced as the gas expands.

The shell has not expanded much by the time the explosive is completely detonated at 35 μs. However, by 43 μs there is some expansion of the shell, more at 65 μs, and still more at 65 μs. At 43 μs some gas has escaped through small cracks in the concrete. More fractures through the structure are evident at 65 μs and the concrete is completely fragmented by 86 μs. Although the simulation extends to 200 μs, well after the latest time shown in Figure 15, we do not show results from later times since these fragments just continue to expand outward.

For the second example, we consider a much larger structure. The structure is a rectangular parallelepiped made of reinforced concrete. The floor slab is 12.192 m by 15.850 m. The walls are placed on top of the slab and are 13.716 m high. The floor slab and walls are 1.8288 m thick. The floor slab is reinforced with #18 rebar at 0.3048-m spacing inside the lower and upper surfaces. The walls are reinforced with #18 rebar at 0.3048-m spacing inside the inner and outer surfaces. The rebar in the walls extends 0.3048 m into the floor slab. The structure is filled with water to a depth of 13.411 m. A cubic yard of explosive is placed on the floor at the middle of the bottom side of one wall. The explosive has a density of 1785.3 kg/m^3 and detonation speed of 8747 m/s. A cubic yard of this explosive has a mass of about 1365.0 kg. It is detonated at time zero at the center of the side in contact with the floor.

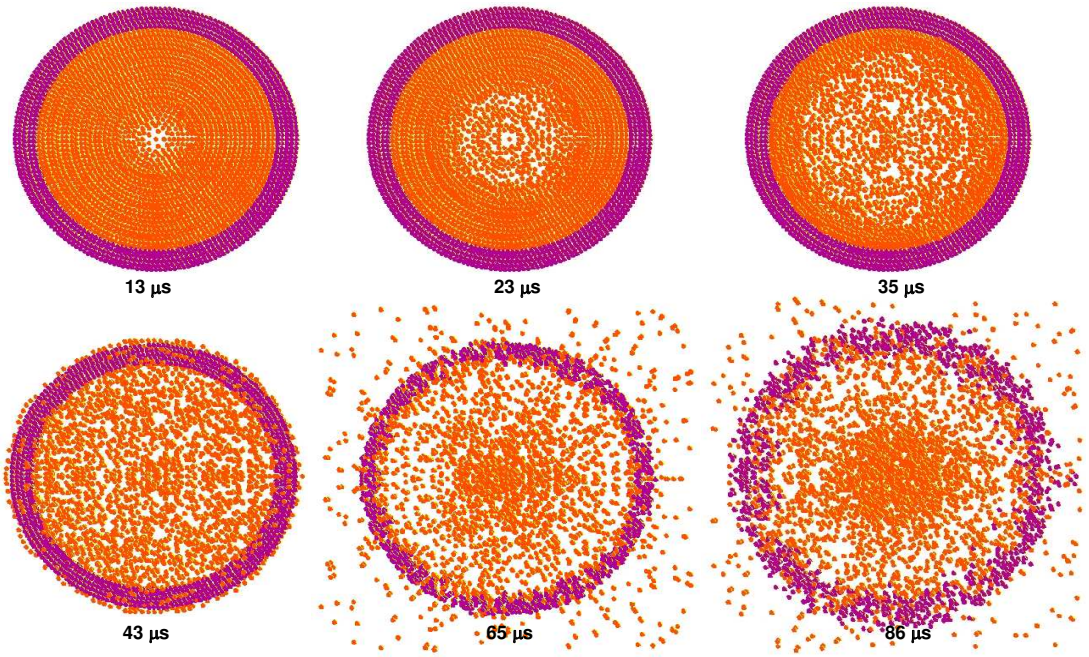

Figure 15. Materials during simulation of exploding concrete shell.

Figure 16 shows results from the EMU simulation of this scenario. In this figure, the concrete is green, the rebar is yellow, the liner is orange, the water is blue, and the explosive is purple. The view is a 0.5-m slice about a symmetry plane through the structure and explosive as shown in the graphic at time zero. The time simulated is about 9.8 ms. The simulation took about 1.52 h using 8 processors, and the time steps varied from 7.4 μs to 13.6 μs. The grid spacing is 0.229 m, and there are 281,032 nodes in the computational model.

The explosive is completely detonated by 0.12 ms, and Figure 16 shows that the region containing the explosive is voided by 0.33 ms. By 1.0 ms, the liner near the initial location of the explosive is fragmented considerably, and by 1.9 ms the outer surface of the floor and concrete wall is slightly bulged near the detonation region. Concrete is leaving the outer surfaces by 2.8 ms as fracturing of the concrete continues. There is no evidence of the liner near the detonation region at this time.

By 4.4 ms, most of the structure is fractured and the detonation gases have reached the surface of the water. Progression of structure damage is evident at the later times shown in this figure at 4.8 ms, 5.3 ms, and 6.3 ms. At 4.8 ms, the liner has been completely removed. By 6.3 ms, all the walls shown in this figure are completely fragmented, and the water is essentially gone. The fragmented materials are dispersing.

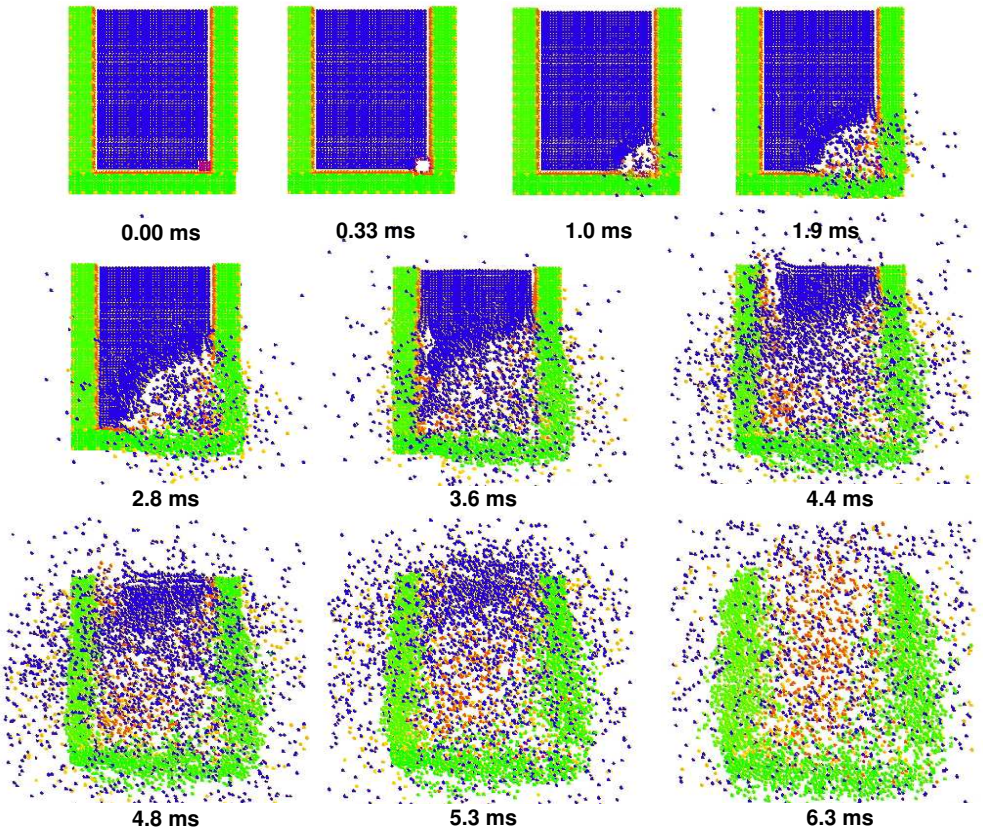

Figure 16. Materials during simulation of detonation within a concrete structure.

Figure 17 shows internal damage to a concrete wall and its rebar reinforcement during the simulation. The wall shown in this figure is adjacent to the explosive and is the wall to the right in Figure 16. No other materials are displayed to obscure the wall. This figure shows damage ranging from no damage (purple) to over 99% damage (orange).

The sequence of times begins at 0.12 ms when the explosive has completely detonated. The damage spreads until by 5.3 ms the bonds in the concrete have completely failed. The spontaneous emergence of cracks is particularly evident in this figure from 1.0 ms until the entire wall is totally fragmented by 5.3 ms. The orange lines in these figures are damage over 99% at the locations of the rebar. They imply that the rebar fails before the concrete.

9. Summary and conclusions

This paper addressed extreme loading of structures using peridynamics. We reviewed peridynamic theory and its implementation in the EMU computer code. The theory as implemented in EMU was illustrated with examples of extreme loadings on reinforced concrete structures by impacts from aircraft. While peridynamic theory has been extended to model composite materials, fluids, and explosives, we discussed only recent developments in modeling gases as peridynamic materials and the detonation model in EMU.

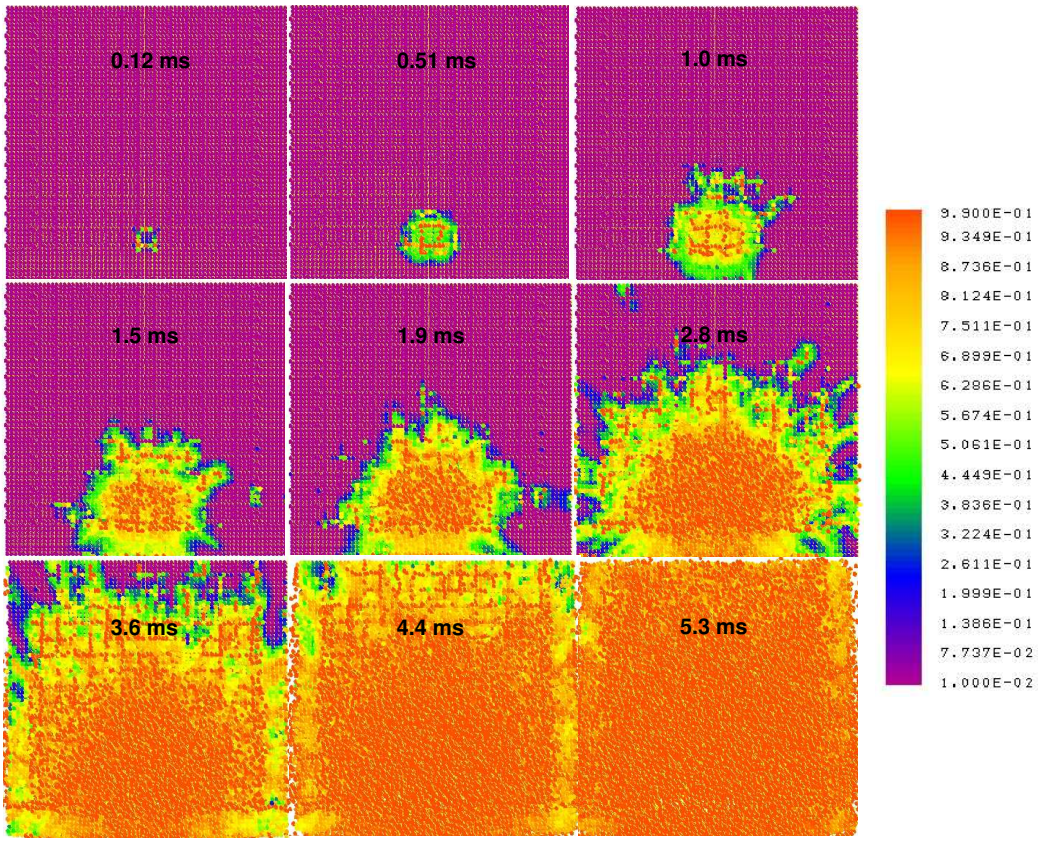

Figure 17. Damage to inside of wall adjacent to explosive.

Explosive loading of concrete structures was then illustrated. The examples illustrate the power of the peridynamics method in problems where deformation and fracture are expected. The work discussed in this paper supports the conclusion that peridynamic theory is a physically reasonable and viable approach to modeling extreme loading of structures from impacts and explosions.

Research and development in peridynamic theory is not completed. We are continuing our research on modeling fluids, composite materials, and explosives. Recently, we extended modeling of gas detonation products to include use of the JWL equation of state [Dobratz and Crawford 1985]. To improve confidence in EMU's capability to model extreme loading, a verification and validation process is being expanded. As the user base and number of code developers increase, attention is being given to software-engineering issues to maintain and distribute the code. There is a long history of constitutive model development to represent stress-strain and yield behavior. We are investigating how this wealth of information can be adapted to the peridynamics paradigm and implemented in EMU.

We envision future research and development addressing problems at both small scales and more encompassing, extreme loading macroscale scenarios. Nanoscale to continuum coupling may be possible using peridynamics with methods such as the embedded atom method [Daw et al. 1993].

Peridynamics has been demonstrated to be viable for analyzing fracture and failure due to loading at the macroscale. We visualize its being viable for analyzing failure at the microscale and nanoscale also. At the macroscale, we see the possibility of including more phenomenology such as fire, heat transfer, material degradation, etc. to provide a more comprehensive methodology for vulnerability assessment of critical structures.

References

[Callen 1960] H. Callen, *Thermodynamics: an introduction to the physical theories of equilibrium thermostatics and irreversible thermodynamics*, Wiley, New York, 1960.

[Cooper 1996] P. W. Cooper, *Explosives engineering*, Wiley-VCH, New York, 1996.

[Daw et al. 1993] M. S. Daw, S. M. Foiles, and M. I. Baskes, "The embedded-atom method: a review of theory and applications", *Mater. Sci. Rep.* **9**:7-8 (1993), 251–310.

[Dayal and Bhattacharya 2006] K. Dayal and K. Bhattacharya, "Kinetics of phase transformations in the peridynamic formulation of continuum mechanics", *J. Mech. Phys. Solids* **54**:9 (2006), 1811–1842.

[Dobratz and Crawford 1985] B. M. Dobratz and P. C. Crawford, "LLNL explosives handbook: properties of chemical explosives and explosive simulants", Technical report, Lawrence Livermore National Laboratory, Livermore, CA., 1985.

[Emmrich and Weckner 2007] E. Emmrich and O. Weckner, "Analysis and numerical approximation of an integro-differential equation modeling non-local effects in linear elasticity", *Math. Mech. Solids* **12**:4 (2007), 363–384. to appear.

[Gerstle and Sau 2004] W. Gerstle and N. Sau, "Peridynamic modeling of concrete structures", pp. 949–956 in *Proceedings of the fifth international conference on fracture mechanics of concrete structures*, vol. 2, edited by L. Li et al., 2004. Ia-FRAMCOS.

[Gerstle et al. 2005] W. Gerstle, N. Sau, and S. Silling, "Peridynamic modeling of plain and reinforced concrete structures", in *18th international conference on structural mechanics in reactor technology (SMiRT 18)*, Beijing, China, 2005. In SMiRT18-B01-2.

[Halliday et al. 2001] D. Halliday, R. Resnick, and J. Walker, *Fundamentals of physics*, vol. 2, 6th ed., Wiley, New York, 2001.

[Hilfer 2000] R. Hilfer (editor), *Applications of fractional calculus in physics*, edited by R. Hilfer, World Scientific, Singapore, 2000.

[Kunin 1982] I. A. Kunin, *Elastic media with microstructure I*, Springer-Verlag, Berlin, 1982.

[Oldham and Spanier 1974] K. B. Oldham and J. Spanier, *The fractional calculus: theory and applications of differentiation and integration to arbitrary order*, Academic, New York, 1974.

[Padilla and Thompson 1984] G. Padilla and S. Thompson, *The RSCORS graphics system*, Albuquerque, NM: Sandia National Laboratories, 1984. SAND83-2639.

[Rogula 1982] D. Rogula (editor), *Nonlocal theory of material media*, edited by D. Rogula, Springer, New York, 1982.

[Silling 2000] S. A. Silling, "Reformulation of elasticity theory for discontinuities and long-range forces", *J. Mech. Phys. Solids* **48**:1 (2000), 175–209.

[Silling 2003] S. A. Silling, "Dynamic fracture modeling with a meshfree peridynamic code", pp. 641–644 in *Computational fluid and solid mechanics*, edited by K. J. Bathe, Elsevier, Amsterdam, 2003.

[Silling and Askari 2005] S. A. Silling and E. Askari, "A meshfree method based on the peridynamic model of solid mechanics", *Comput. Struct.* **83**:17-18 (2005), 1526–1535.

[Silling and Bobaru 2005] S. A. Silling and F. Bobaru, "Peridynamic modeling of membranes and fibers", *Int. J. Nonlinear Mech.* **40**:2-3 (2005), 395–409.

[Silling et al. 2003] S. A. Silling, M. Zimmermann, and R. Abeyaratne, "Deformation of a peridynamic bar", *J. Elasticity* **73**:1-3 (2003), 173–190.

[Sugano et al. 1993] T. Sugano, H. Tsubota, Y. Kasai, N. Koshika, S. Orui, W. A. von Riesemann, D. C. Bickel, and M. B. Parks, "Full-scale aircraft impact test for evaluation of impact force", *Nucl. Eng. Des.* **140**:3 (1993), 373–385.

[Weckner and Abeyaratne 2005] O. Weckner and R. Abeyaratne, "The effect of long-range forces on the dynamics of a bar", *J. Mech. Phys. Solids* **53**:3 (2005), 705–728.

[Young 1969] C. W. Young, "Depth predictions for earth penetrating projectiles", *J. Soil Mech. Found. Div.* **95**:SM3 (1969), 803–817.

Received 21 May 2007. Accepted 23 May 2007.

PAUL N. DEMMIE: pndemmi@sandia.gov
Multiscale Dynamic Material Modeling Department, Sandia National Laboratories, Box 5800 MS 1322, Albuquerque, NM 87185-1322, United States

STEWART A. SILLING: sasilli@sandia.gov
Multiscale Dynamic Material Modeling Department, Sandia National Laboratories, Box 5800 MS 1322, Albuquerque, NM 87185-1322, United States